

CrossMark  
click for updatesCite this: *J. Mater. Chem. A*, 2015, 3,  
18839Received 22nd July 2015  
Accepted 18th August 2015

DOI: 10.1039/c5ta05594f

www.rsc.org/MaterialsA

## Self-template synthesis of hollow shell-controlled $\text{Li}_3\text{VO}_4$ as a high-performance anode for lithium-ion batteries†

Qidong Li,‡ Qiulong Wei,‡ Qinqin Wang, Wen Luo, Qinyou An, Yanan Xu,  
Chaojiang Niu, Chunjuan Tang and Liqiang Mai\*

A hollow shell-controlled  $\text{Li}_3\text{VO}_4$  is fabricated *via* a facile self-template method, which has a controllable shell thickness in the range of 10–300 nm. This hollow shell-controlled  $\text{Li}_3\text{VO}_4$  composited with reduced graphene oxide exhibits excellent rate capability (201 mA h g<sup>-1</sup> at 125 C) and superior high-temperature stability (364.2 mA h g<sup>-1</sup> after 1000 cycles at 10 C, 60 °C).

Lithium-ion batteries (LIBs) have been one of the most important energy-storage devices because of their many merits, such as high energy density, high power density and environmental benignity.<sup>1</sup> They have been recently regarded as promising power sources for electric vehicles (EVs) and hybrid electric vehicles (HEVs) as well as for portable electronic devices.<sup>2</sup> However, for EVs and HEVs, the key safety issue in LIBs is the lithium dendrite growth on the commercial graphite surface during the charging–discharging process.<sup>3</sup>  $\text{Li}_4\text{Ti}_5\text{O}_{12}$  (LTO) has been considered as the most promising one to replace graphite because of its high stability, rate capability, and safety based on a relatively high potential (1.5 V *vs.* Li<sup>+</sup>/Li),<sup>4</sup> but its intrinsically low theoretical capacity (175 mA h g<sup>-1</sup>) prevents its widespread use in LIBs.

Recently,  $\text{Li}_3\text{VO}_4$  (LVO), as a solid ionic-conductor, has emerged as an alternative to LTO since several studies have shown its potential as a promising anode for LIBs.<sup>5–12</sup> LVO has a theoretical capacity of 394 mA h g<sup>-1</sup> when lithiated to  $\text{Li}_3\text{VO}_4$ :  $\text{Li}_3\text{VO}_4 + x\text{Li}^+ + 2e^- \leftrightarrow \text{Li}_{3+x}\text{VO}_4$  ( $x = 2$ ), whose capacity is higher than that of LTO.<sup>8</sup> Moreover, the appropriate operating voltage (0.5–0.8 V *vs.* Li<sup>+</sup>/Li) avoids the formation of lithium dendrites and guarantees high voltage and high energy density of the full cell. Owing to its potential in LIBs, many approaches such as carbon material compositing, hollow structure construction and particle size

reduction to the nanoscale have been carried out to prompt the real application of LVO.<sup>7,8,10–13</sup> However, the microstructure of LVO synthesized by previous methods, such as the solid state method and high-temperature hydrothermal method,<sup>5,8,9</sup> is not feasible to be controlled over size, shape and dimensionality which are closely related to the electrochemical performances of LVO. For its wide applications, a controllable structure with mild reaction conditions for LVO is of great significance in the improvement of its electrochemical performance.

Herein, we first report a novel and facile self-template method to synthesize the  $\text{Li}_3\text{VO}_4$ /reduced graphene oxide hollow shell (denoted as LVO/rGO-HS). The synthesis involves a facile oil-bath synthesis of core–shell solid particles in a mixed solvent ( $\text{H}_2\text{O}$  and ethylene glycol (EG)) and subsequent core removal by water to form LVO/rGO-HS. Importantly, the resulting LVO/rGO-HS can be easily controlled by varying the ratio between the  $\text{H}_2\text{O}$  and EG in the mixed solvent. When used as anodes for LIBs, the thinnest LVO/rGO-HS exhibits superior rate capability and excellent high-temperature cycling stability. Moreover, the pseudocapacitive behavior of LVO has been first analyzed at different operating temperatures.

LVO can be synthesized in  $\text{H}_2\text{O}$  (denoted as LVO-H) and EG (denoted as LVO-EG) through the same oil-bath method. These two as-prepared samples possess different physicochemical properties. The nucleation temperature of LVO-EG is about 75 °C in EG, lower than that of LVO-H in  $\text{H}_2\text{O}$  (85 °C). The XPS spectra confirm the presence of tetravalent vanadium ions (516.3 eV) in LVO-EG, which indicate the existence of oxygen vacancies in it (Fig. S1†).<sup>13</sup> For LVO, it is built up of oxygen atoms in approximately hexagonal close packing and the cations occupy ordered tetrahedral sites.<sup>5</sup> The large number of oxygen vacancies leads to the higher solubility of LVO-EG in water than that of LVO-H. Based on the above results, we first designed a LVO-EG/LVO-H core–shell structure in a mixed solvent (denoted as LVO-M), and then removed the LVO-EG core to form a LVO hollow shell. The whole formation process of LVO-M can be generally divided into four stages as schematically illustrated in Fig. 1a. In stage I, the LVO-EG is nucleated

State Key Laboratory of Advanced Technology for Materials Synthesis and Processing, Wuhan University of Technology, Wuhan 430070, China. E-mail: mlq518@whut.edu.cn

† Electronic supplementary information (ESI) available. See DOI: 10.1039/c5ta05594f

‡ These authors contributed equally to this work.

and grown first in the mixed solvent. Then with increasing temperature, the LVO-H is nucleated on the surface of the LVO-EG, as shown in stage II. These crystal nuclei of LVO-H will grow up to form the shell as time goes on, as shown in stage III and stage IV.

To illustrate the formation mechanism of the core-shell LVO-M, scanning electron microscopy (SEM) is conducted to monitor the morphological evolution and crystallization process with increasing reaction time. It can be seen from Fig. 1b, that after 8 min, the LVO-EG is composed of spherical particles with a smooth surface. After 10 min, the LVO-H begins nucleating on the surface of LVO-EG (Fig. 1c). As time goes on, the small crystal nuclei of LVO-H grow up to larger particles and connect with each other (Fig. 1d). At the end of the reaction, the LVO-H shell is formed and coats on the LVO-EG (Fig. 1e).

Moreover, graphene oxide (GO) was introduced to further improve the electronic conductivity and prevent the agglomeration of LVO particles. Fig. 1f shows the morphology of LVO-M with the introduction of GO (denoted as LVO-M/rGO). The LVO-M/rGO particles are more uniform and smaller compared with the LVO-M. Water is used to remove the LVO-EG core, and then the LVO/rGO-HS is obtained (Fig. 1g). From the XRD pattern (Fig. S2<sup>†</sup>), the diffraction peaks of LVO-M are the merge of that of the LVO-EG and LVO-H, which demonstrate the coexistence of LVO-EG and LVO-H. The TEM image (Fig. S3<sup>†</sup>) clearly shows the core-shell structure of LVO-M/rGO.

This hollow shell can be easily controlled by adjusting the volume ratio of water and EG in the mixed solvent. LVO/rGO-HS-1/2/3/4 samples exhibit different particle sizes and hollow morphologies, as shown in Fig. 2 and S4.<sup>†</sup> LVO/rGOHS-1 is synthesized with a 3 : 1 volume ratio of water and EG (Fig. 2a, d and g). The hollow shell is inconspicuous in the SEM images because of the thick shell. The thickness of the LVO/rGO-HS-1 shell is about 300 nm (Fig. 2g). For LVO/rGO-HS-2 (the volume ratio of water and EG is 1 : 1, Fig. 2b, e and h), the hollow shell is

more obvious and uniform. The TEM image shows that the thickness of the LVO/rGO-HS-2 sample shell is around 40–80 nm. The LVO/rGO-HS-3 sample (the volume ratio of water and EG is 1 : 3, Fig. 2c and f) shows a thinner shell which is around 10–30 nm, and many shells are broken during the LVO-EG removal process because of the thin shell. With more EG in the solvent, LVO/rGO-HS-4 (the volume ratio of water and EG is 1 : 7, Fig. S4a and b<sup>†</sup>), the spherical shell would be disintegrated in the LVO-EG removal process. The elemental analysis results confirm that the amount of carbon in LVO/rGO-HS-1/2/3/4 is 1.70%, 3.15%, 4.88% and 9.86%, respectively. The above investigation confirms that the volume ratio of water and EG has a significant impact on the hollow shell morphology. Within a certain range, the larger ratio of EG in the mixed solvent contributes to an expected and uniform hollow shell with a thinner shell (from ~300 nm to 10 nm Fig. 2g–i) and smaller particle size (from 1.2 μm to 400 nm, Fig. 2g–i), whereas too much EG in the mixed solvent limits the formation of LVO-H, and prevents the formation of the hollow shell.

The different morphologies of LVO/rGO-HS-1/2/3 samples result in their different electrochemical performances. The lithium storage performances of these three samples are evaluated in a potential window of 0.2–3 V *versus* Li<sup>+</sup>/Li. The typical charge–discharge profiles of the LVO/rGO-HS-3 sample at 0.25 C are shown in Fig. S5,<sup>†</sup> which are consistent with those results previously reported.<sup>5–13</sup> Fig. 3a shows the cyclic performance and corresponding coulombic efficiency over 1500 cycles at a 10 C (4 A g<sup>−1</sup>). The capacity retention of the LVO/rGO-HS-1, LVO/rGO-HS-2, and LVO/rGO-HS-3 electrodes at the end of the cycling test is 72% (163.6 mA h g<sup>−1</sup>), 43% (137.6 mA h g<sup>−1</sup>), and 75% (257.9 mA h g<sup>−1</sup>), respectively. The coulombic efficiencies of the three samples are nearly 100% after a few cycles and the high value is maintained afterwards. Among them, the LVO/rGO-HS-2 and LVO/rGO-HS-3 samples show high specific capacity in the first few cycles. This could be ascribed to the thin

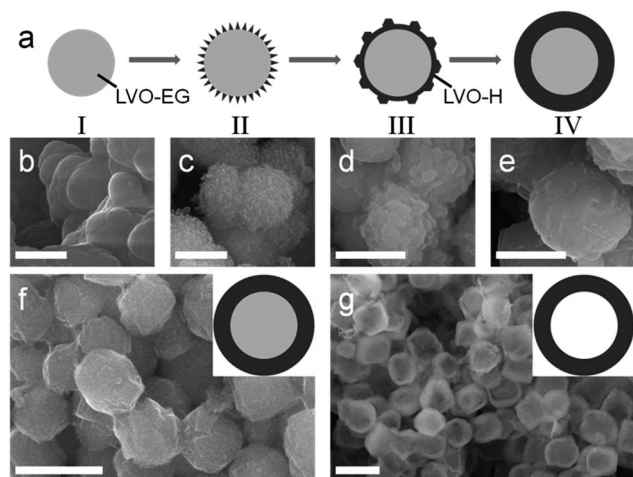


Fig. 1 (a) The formation mechanism of LVO-M; SEM images of the production without GO at 120 °C for 8 min (b), 10 min (c), 10.5 min (d), and 30 min (e); the volume ratio of H<sub>2</sub>O and EG is 1 : 1; (f) SEM image of LVO-M/rGO; (g) SEM image of LVO/rGO-HS. Scale bar 1 μm.

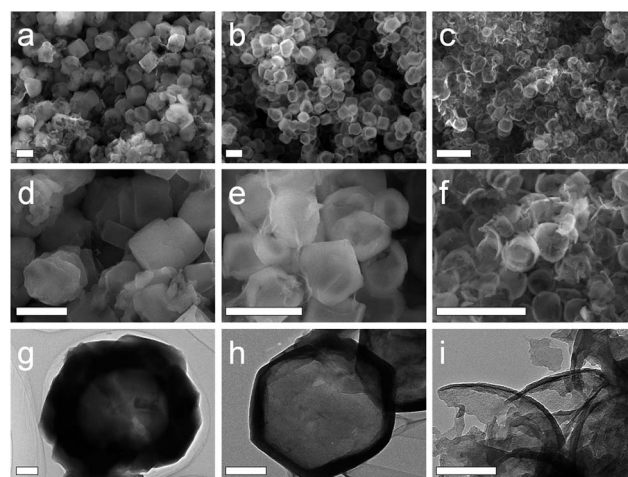


Fig. 2 The SEM images of LVO/rGO-HS-1 (a and d); the SEM images of the LVO/rGO-HS-2 (b and e); the SEM images of the LVO/rGO-HS-3 (c and f); scale bar 1 μm. The TEM images of LVO/rGO-HS-1 (g), LVO/rGO-HS-2 (h), and LVO/rGO-HS-3 (i), respectively. Scale bar 200 nm.

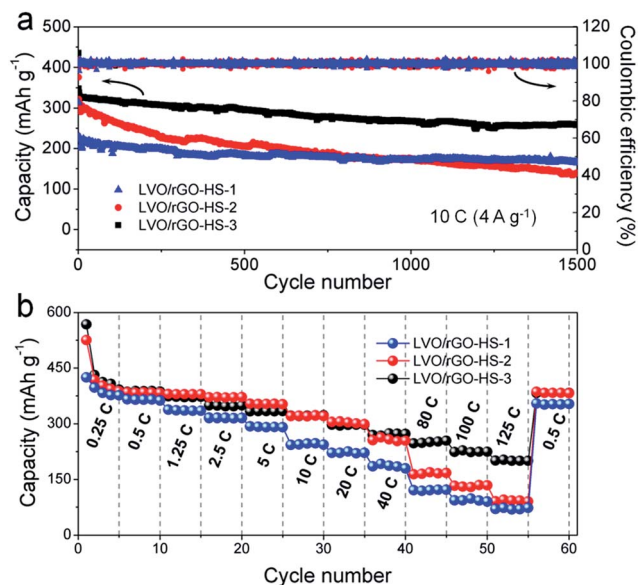


Fig. 3 (a) Cycling performances and coulombic efficiencies of LVO/rGO-HS-1/2/3 at 10 C; (b) rate capabilities of LVO/rGO-HS-1/2/3.

shell which reduces the diffusion distance of Li<sup>+</sup>. But for the LVO/rGO-HS-2 sample, the intact hollow shell with the closed thin shell may be destroyed in the following cycles, resulting in fast capacity fading.<sup>14</sup> For the LVO/rGO-HS-3 sample, the broken spherical shells provide an opening edge to release the stress during the charging–discharging process, leading to the excellent cycling stability at high rate.<sup>14</sup> The thick shell of the LVO/rGO-HS-1 sample with good mechanical robustness makes it exhibit good cycling stability but low specific capacity. Moreover, improvement in the rate performance is also achieved for the hollow shell electrode, as shown in Fig. 3b. As expected, the LVO/rGO-HS-3 electrode with the thinnest shell displays the best rate capability.<sup>15–18</sup> Specifically, even at an extremely high rate of 125 C, the specific capacity still can achieve 201 mA h g<sup>-1</sup>, higher than the theoretical capacity of LTO. This is the best

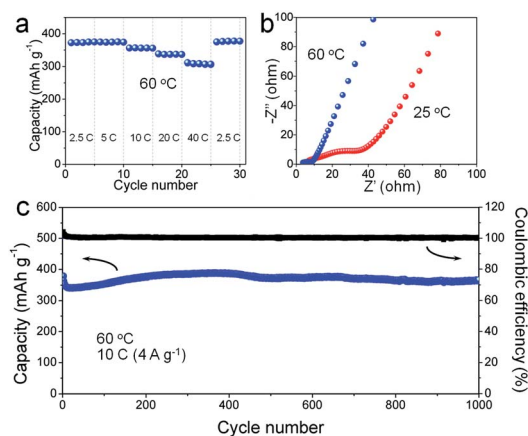


Fig. 4 (a) Rate capability of LVO/rGO-HS-3 at 60 °C; (b) EIS spectra of LVO/rGO-HS-3 at 25 and 60 °C after 20 cycles; (c) cycling performance and coulombic efficiency of LVO/rGO-HS-3 at 60 °C.

rate performance among the published LVO/carbon composite based anode (Table S1†).<sup>7,8,10–13</sup> The rate performances of solid LVO/rGO, LVO-HS-3 and solid LVO are shown in Fig. S6.† The comparison of these three samples confirms that the construction of a hollow structure and the introduction of rGO significantly improve the electrochemical performances of LVO.

In the case of a promising practical electrode material, the electrochemical performance at high temperature is another crucial factor. To assess the performance of our material, we selected aggressive tests where the LVO/rGO-HS-3 electrode is cycled at a temperature of 60 °C. Apparently, the capacities increase from 347 to 374, 333 to 374, 316 to 357, 296 to 337, and 270 to 309 mA h g<sup>-1</sup> with increasing temperature from 25 to 60 °C at the rates of 2.5, 5, 10, 20, and 40 C, respectively (Fig. 4a). The impressive enhanced capacities attribute to the significantly reduced contact and charge-transfer resistances in LVO/rGO-HS-3 architecture at higher temperature, according to the EIS spectra (Fig. 4b).<sup>19</sup> To further understand the influence of temperature on our material, increasing voltammetric scan rates at 25 °C and 60 °C are used to identify the contribution of capacitive behavior and faradaic reaction. The total current response (*i*) at a fixed potential (*V*) can be separated into two mechanisms, according to the following equation:

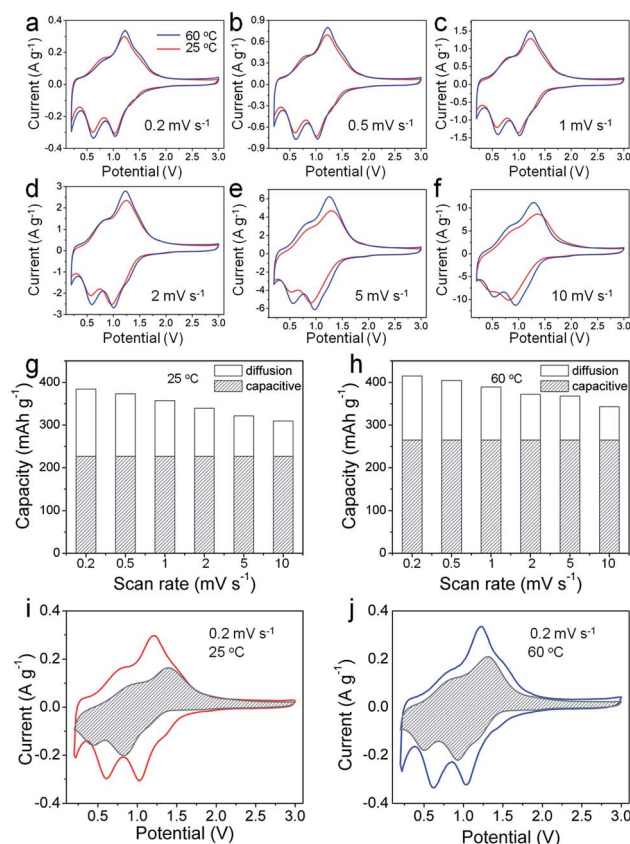


Fig. 5 (a–f) The CV curves of the LVO/rGO-HS-3 electrode at different scan rates at different temperatures; (g and h) the contribution of capacitive and insertion processes to the total capacities at different scan rates at different temperatures; (i and j) capacitive and diffusion-controlled charge storage contributions separated with a cyclic voltammogram at 0.2 mV s<sup>-1</sup> at different temperatures.

$$i(V) = k_1v + k_2v^{1/2} \quad (1)$$

where  $k_1v$  corresponds to the capacitive contribution, and  $k_2v^{1/2}$  stands for the contribution of the diffusion-controlled faradaic intercalation process.<sup>20–22</sup> From the cyclic voltammetry (CV) curves, the polarization of the LVO/rGO-HS-3 electrode has been reduced at high temperature (Fig. 5a–f), which coincides well with the EIS results. Fig. 5g and h show the contribution of capacitive and insertion processes to the total capacities at different scan rates. Notably, the enhancements of the total capacities almost result from the increase of pseudocapacitive contribution at high temperature, from 226 to 265 mA h g<sup>-1</sup>. In Fig. 5i and j, the shaded areas correspond to the voltage curve for the capacitive current response in comparison with the total measured current at a scan rate of 0.2 mV s<sup>-1</sup> at 25 and 60 °C, respectively. Apparently, the Li<sup>+</sup> insertion capacities are observed at peak potential and the nondiffusion-controlled processes dominate the rest of the potentials.<sup>23</sup> More remarkably, even at a high temperature of 60 °C, the LVO/rGO-HS-3 electrode shows a superior capacity retention of 364.2 mA h g<sup>-1</sup> after 1000 cycles at 10 C (Fig. 4c). The impressive results demonstrate that the LVO/rGO-HS-3 electrode can provide fast discharging and charging capability with high capacity and long cycling performance even at high temperature.

## Conclusions

In conclusion, a hollow shell-controlled LVO/rGO structure is successfully designed and synthesized *via* a facile oil-bath method. The thickness of the hollow shell can be easily controlled ranging from 10–300 nm by adjusting the volume ratio of water and EG in the solvent. The thinnest LVO/rGO-HS displays a specific capacity of 387 mA h g<sup>-1</sup> at 0.5 C and stable cycling performance with 75% retention over 1500 cycles at 10 C. Remarkably, an impressive capacity of 201 mA h g<sup>-1</sup> is achieved at an extremely high rate of 125 C. Moreover, even at high temperatures, the LVO/rGO-HS-3 delivers excellent rate capability and superior cycling performance. The superior electrochemical performances are attributed to the reduced Li<sup>+</sup> ion diffusion pathway originated from the optimized hollow shell, the enhanced electronic conductivity arose from the introduction of rGO and the structure stability brought by the opening edge. We believe that this material with superior electrochemical performances and a facile synthesis method will be a promising practical anode for high power LIBs.

## Acknowledgements

This work was supported by the National Basic Research Program of China (2013CB934103, 2012CB933003), the International Science and Technology Cooperation Program of China (2013DFA50840), the National Science Fund for

Distinguished Young Scholars (51425204), the Hubei Province Natural Science Fund for Distinguished Young Scholars (2014CFA035), and the Fundamental Research Funds for the Central Universities (2014-YB-001). Thanks to Prof. D. Y. Zhao of Fudan University and Prof. C. M. Lieber of Harvard University for their strong support and stimulating discussions.

## Notes and references

- 1 M. Armand and J.-M. Tarascon, *Nature*, 2008, **451**, 652.
- 2 M. Galinski, K. Babel and K. Jurewicz, *J. Power Sources*, 2013, **228**, 83.
- 3 S. S. Zhang, *J. Power Sources*, 2006, **161**, 1385.
- 4 J. B. Goodenough and Y. Kim, *Chem. Mater.*, 2009, **22**, 587.
- 5 H. Li, X. Liu, T. Zhai, D. Li and H. Zhou, *Adv. Energy Mater.*, 2013, **3**, 428.
- 6 S. Ni, X. Lv, J. Ma, X. Yang and L. Zhang, *J. Power Sources*, 2014, **248**, 122.
- 7 Q. Li, J. Sheng, Q. Wei, Q. An, X. Wei, P. Zhang and L. Mai, *Nanoscale*, 2014, **6**, 11072.
- 8 Y. Shi, J.-Z. Wang, S.-L. Chou, D. Wexler, H.-J. Li, K. Ozawa, H.-K. Liu and Y.-P. Wu, *Nano Lett.*, 2013, **13**, 4715.
- 9 W.-T. Kim, Y. U. Jeong, Y. J. Lee, Y. J. Kim and J. H. Song, *J. Power Sources*, 2013, **244**, 557.
- 10 Z. Jian, M. Zheng, Y. Liang, X. Zhang, S. Gheyhani, Y. Lan, Y. Shi and Y. Yao, *Chem. Commun.*, 2015, **51**, 229.
- 11 Z. Liang, Z. Lin, Y. Zhao, Y. Dong, Q. Kuang, X. Lin, X. Liu and D. Yan, *J. Power Sources*, 2015, **274**, 345.
- 12 J. Liu, P.-J. Lu, S. Liang, W. Wang, M. Lei, S. Tang and Q. Yang, *Nano Energy*, 2015, **12**, 709.
- 13 C. Zhang, H. Song, C. Liu, Y. Liu, C. Zhang, X. Nan and G. Cao, *Adv. Funct. Mater.*, 2015, **25**, 3497.
- 14 X. W. D. Lou, L. A. Archer and Z. Yang, *Adv. Mater.*, 2008, **20**, 3987.
- 15 Z. Wang and L. Zhou, *Adv. Mater.*, 2012, **24**, 1903.
- 16 S. Ding, D. Zhang, H. B. Wu, Z. Zhang and X. W. D. Lou, *Nanoscale*, 2012, **4**, 3651.
- 17 G. Zhang, H. B. Wu, T. Song, U. Paik and X. W. D. Lou, *Angew. Chem., Int. Ed.*, 2014, **53**, 12590.
- 18 L. Zhou, D. Zhao and X. W. Lou, *Adv. Mater.*, 2012, **24**, 745.
- 19 L. Mai, Q. Wei, Q. An, X. Tian, Y. Zhao, X. Xu, L. Xu, L. Chang and Q. Zhang, *Adv. Mater.*, 2013, **25**, 2969.
- 20 V. Augustyn, J. Come, M. A. Lowe, J. W. Kim, P.-L. Taberna, S. H. Tolbert, H. D. Abruña, P. Simon and B. Dunn, *Nat. Mater.*, 2013, **12**, 518.
- 21 M. Park, X. Zhang, M. Chung, G. B. Less and A. M. Sastry, *J. Power Sources*, 2010, **195**, 7904.
- 22 D. Baronetto, N. Krstajić and S. Trasatti, *Electrochim. Acta*, 1994, **39**, 2359.
- 23 M. Sathiyaa, A. Prakash, K. Ramesha, J. M. Tarascon and A. Shukla, *J. Am. Chem. Soc.*, 2011, **133**, 16291.